

Supporting Information for

**Oxygen-Deficient WO₃ via High-Temperature Two-Step Annealing for
Enhanced and Stable Water Splitting**

Shasha Tang,¹ Marc Courté,¹ Jingjing Peng,² and Denis Fichou.^{1,3*}

¹School of Physical and Mathematical Sciences, Nanyang Technological University, 637371, Singapore

²Beijing Institute of Aeronautical Materials, Beijing, 100095, P. R. China

³Sorbonne Université, CNRS, Institut Parisien de Chimie Moléculaire (UMR 8232), 4 Place Jussieu, 75005 Paris, France

*Corresponding Author: E-mail: denisfichou@ntu.edu.sg

1. Experimental Section

a. Synthesis of WO₃ Plates

The WO₃ plate was synthesized by a combining technique of hydrothermal treatment and two-step annealing treatment. First, the commercial tungsten foil was sonication cleaned with ethanol and de-ionized (DI) water for 15 min each. After drying with a nitrogen gas gun, the tungsten foil was immersed in a Teflon liner containing 50 mL DI water of 1.5 M nitric acid and 80 mg ammonium fluoride. Then, the Teflon liner was put in the stainless steel autoclave and heated at 150°C for 3 hours. After cooling down naturally, the fabricated yellow precursor was washed with DI water and dried in an oven at 60°C for 5 hours.

In the first annealing treatment, the yellow precursor was heated up from room temperature to 550°C in 30 min and annealed at 550°C for different duration (1-6 hours) in air. This turned the yellow precursor blue, suggesting the formation of WO₃. Here, we chose the sample annealed at 550°C for 3 hours and denoted it as WO₃-S0.

In order to obtain oxygen-deficient WO₃, the above blue WO₃-S0 sample was annealed again in air. The heating rate was 3°C per minute for the second annealing process. The samples annealed again at 700°C for 60 min were denoted as WO₃-S1. After the second annealing treatment, the blue sample became olive yellow.

To make a supplement, the samples second annealed at 670°C for 30 min, 700°C for 30 min, are denoted as WO₃-S2, and WO₃-S3, respectively.

b. Material Characterization

Field emission scanning electron microscopy (FESEM, JEOL JSM-6700F) and transmission electron microscopy (TEM, JEOL JEM-2100PLUS) was used to characterize the morphology of WO₃ samples. The sample chemical compositions were confirmed by X-ray diffraction (XRD, Bruker D2 Phaser). The chemical valence states and oxygen vacancies of WO₃ samples were measured by X-ray photoelectron spectroscopy (XPS) with a Thermo Fisher ESCALAB 250Xi machine. Room temperature Raman measurements measurement were utilized to investigate

the structure change and performed with a WITec CRM 200 system (an excitation laser with a wavelength of 532 nm). UV-vis spectrophotometer (UV-3600, Shimadzu) was used to record the diffuse reflectance spectra (DRS) of the WO₃ samples. In order to obtain the band gap, Kubelka–

Munk function ($F(R) = \frac{(1 - R)^2}{2R}$, where R is the reflectance) is used to calculate the absorption coefficient F(R). After that, we can determine the Tauc Plots (F(R)·hv^{1/2} vs. hv) based on F(R). Then, the slope of the curves in Tauc Plots is the band gap of WO₃. The WO₃ samples were characterized by photoluminescence (FluoroMAX-4, Horiba scientific).

c. Photoelectrochemical Measurements

Photoelectrochemical measurements were performed by an Autolab electrochemical workstation coupled to a Newport solar simulator (AM 1.5) at room temperature. The WO₃ samples were used as working electrodes, a platinum foil as the counter electrode, and an Ag/AgCl (3.0 M KCl) electrode as the reference. All electrodes were immersed into the 0.5 M Na₂SO₄ electrolyte in a three-electrode quartz glass configuration. Then, linear sweep voltammetry (LSV) tests were performed at 10 mV s⁻¹ under incident chopped light (f = 0.1 Hz). The stability tests were investigated at constant voltage (1.51 V vs. RHE) by chronopotentiometry method. The short-term stability tests were recorded under incident chopped light (f = 0.05 Hz, AM 1.5) for 600s. Then, the above samples were used to perform the long-term stability tests with a chopped light (f = 0.05 Hz, AM 1.5) for 600s every 2 hours or 12 hours, and tested for 24 hours in total. The current density was calculated based on the geometric area of the electrode. The amount of evolved H₂ gas and the faradaic efficiency was measured with at the potential of 1.51 V vs. RHE for 60 min by a gas chromatography (Agilent 7890B with a TCD detector). The incident photon to current conversion efficiency (IPCE) was measured at 1.23 V vs. RHE via the electrochemical workstation coupled to the light source with band-pass filters. A Newport 1919-R optical power meter was used to record the monochromatic light intensity. IPCE is expressed by the equation: $IPCE = (1240 * I) / (\lambda * P)$, where I is the photocurrent density (mA cm⁻²) under the monochromatic light, λ and P are the wavelength (nm) and intensity (mW cm⁻²) of the light,

respectively. Electrochemical impedance spectroscopy (EIS) was performed at the potential of 1.0 V vs. RHE with the AC amplitude of 10 mV under light illumination. The frequency range is from 0.1 Hz to 10 kHz. The applied bias photon-to-current efficiency (ABPE) was calculated

$$\frac{J_{ph} \times |1.23 - V_{app}|}{P_{total}} \times 100$$

following the equation: ABPE (%) = $\frac{J_{ph} \times |1.23 - V_{app}|}{P_{total}} \times 100$, where J_{ph} and V_{app} are the photocurrent density (mA cm^{-2}) and applied bias (V) while P_{total} means the incident illumination power density (100 mW cm^{-2}). In all measurements, Ag/AgCl (3.0 M KCl) electrode was used as the reference, which has the potential of 0.210 V vs. RHE. The pH value of 0.5 M Na_2SO_4 electrolyte was 5.16 and double detected by both the pH Test Strip and the pH Meter (OHAUS-Starter 3100 Bench pH Meter). Potentials obtained in this study were calibrated against the reversible hydrogen electrode (RHE) reference by the following Nernst equation: $E (\text{V vs. RHE}) = E (\text{V vs. Ag/AgCl}) + 0.059 \text{ pH} + E (\text{Ag/AgCl vs. RHE})$. The catalytic area of our samples is 1 cm^{-2} .

Table S1: Light intensity for IPCE calculation

wavelength (nm)	300	310	320	330	340	350	360	370	380	390
light intensity (mW cm^{-2})	0.010	0.012	0.013	0.017	0.022	0.026	0.028	0.029	0.032	0.037
wavelength (nm)	400	410	420	430	440	450	460	470	480	490
light intensity (mW cm^{-2})	0.043	0.043	0.045	0.054	0.067	0.082	0.105	0.129	0.118	0.120
wavelength (nm)	500	520	540	560	580	600				
light intensity (mW cm^{-2})	0.118	0.119	0.122	0.121	0.122	0.116				

2. Figures and captions

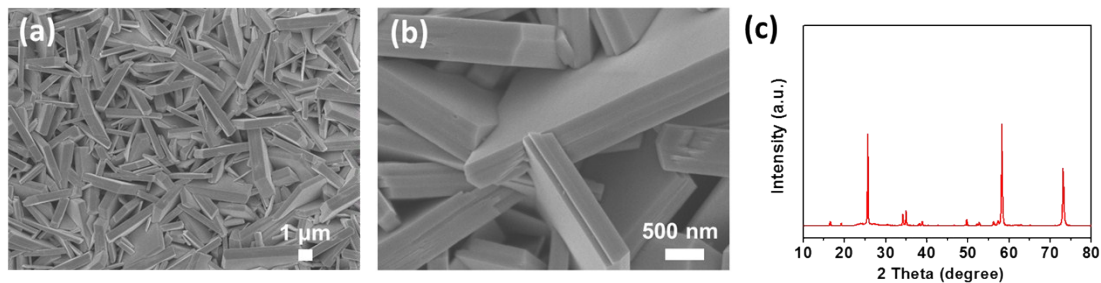


Figure S1 Different magnification SEM images (a,b) and XRD pattern (c) of the WO₃ precursor after hydrothermal process. The scale bar corresponds to 1 μm (a) and 500 nm (b).

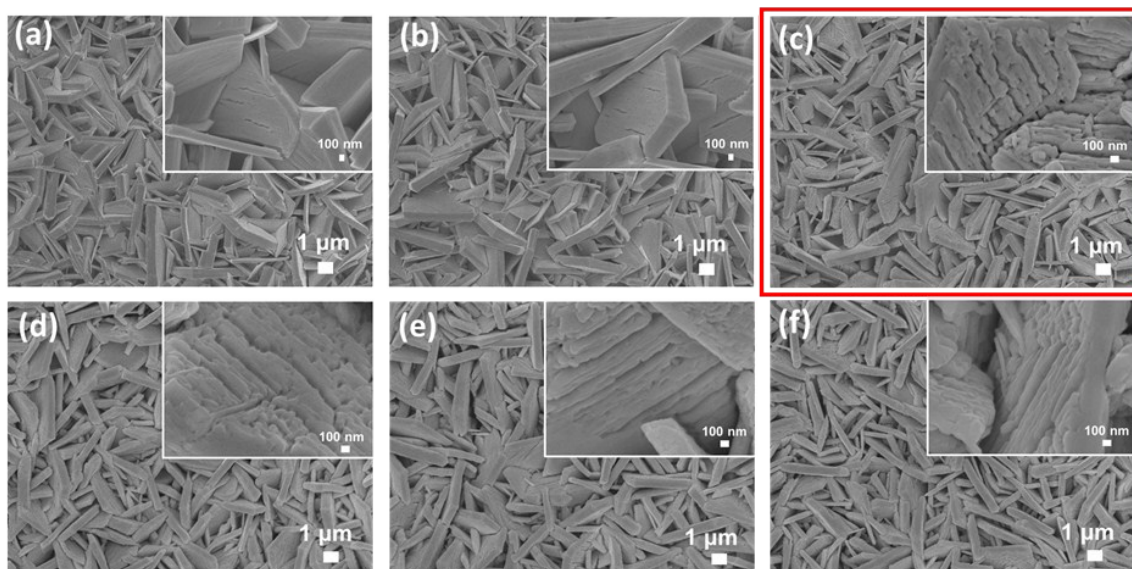


Figure S2 SEM images reveal morphological differences among the WO₃ samples only annealed at 550°C for different duration. (a) 1 hour, (b) 2 hours, (c) 3 hours, (d) 4 hours, (e) 5 hours, and (f) 6 hours, respectively. The inserts are the corresponding high magnification images of above samples.

When we perform a conventional one-step annealing process with the precursor at 550°C for different duration, the morphology experiences a huge variation. It is visible that some smooth plates are ruptured after 1 and 2 hours annealing. When the heating time prolongs to 3 hours, more plates tend to be ruptured and small particles are formed on the surface. However, when the time exceeds 3 hours, the morphology is almost preserved and remains the same as the 3 hours sample. This is one reason that sample annealed at 550°C for 3 hours is chosen and denoted it as WO₃-S0.

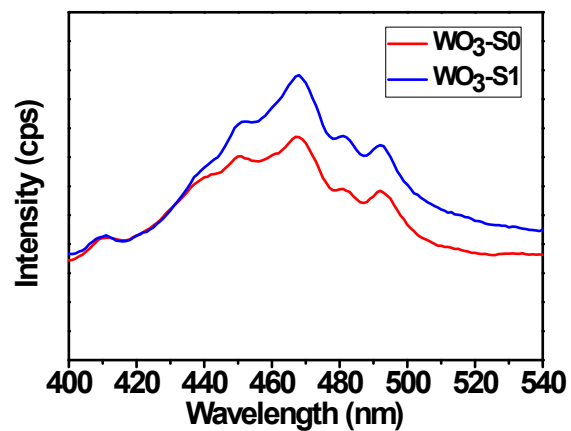


Figure S3 Photoluminescence spectroscopy (PL) of $\text{WO}_3\text{-S0}$ and $\text{WO}_3\text{-S1}$ samples.

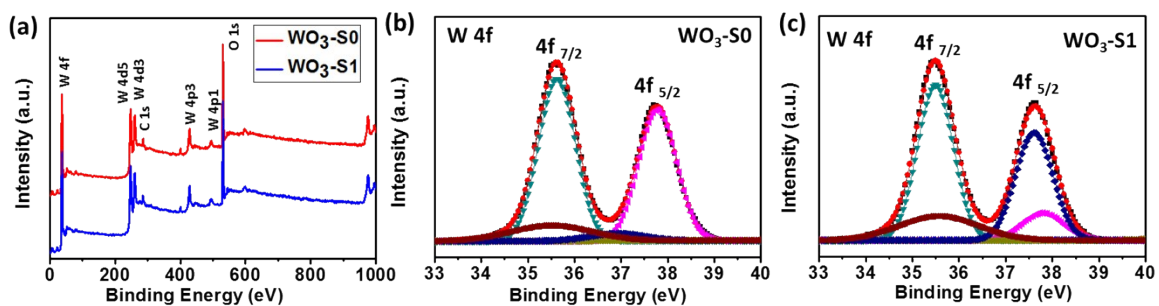


Figure S4 (a) The full survey spectra of XPS measurements of $\text{WO}_3\text{-S0}$ and $\text{WO}_3\text{-S1}$. XPS W 4f spectra of $\text{WO}_3\text{-S0}$ (b) and $\text{WO}_3\text{-S1}$ (c).

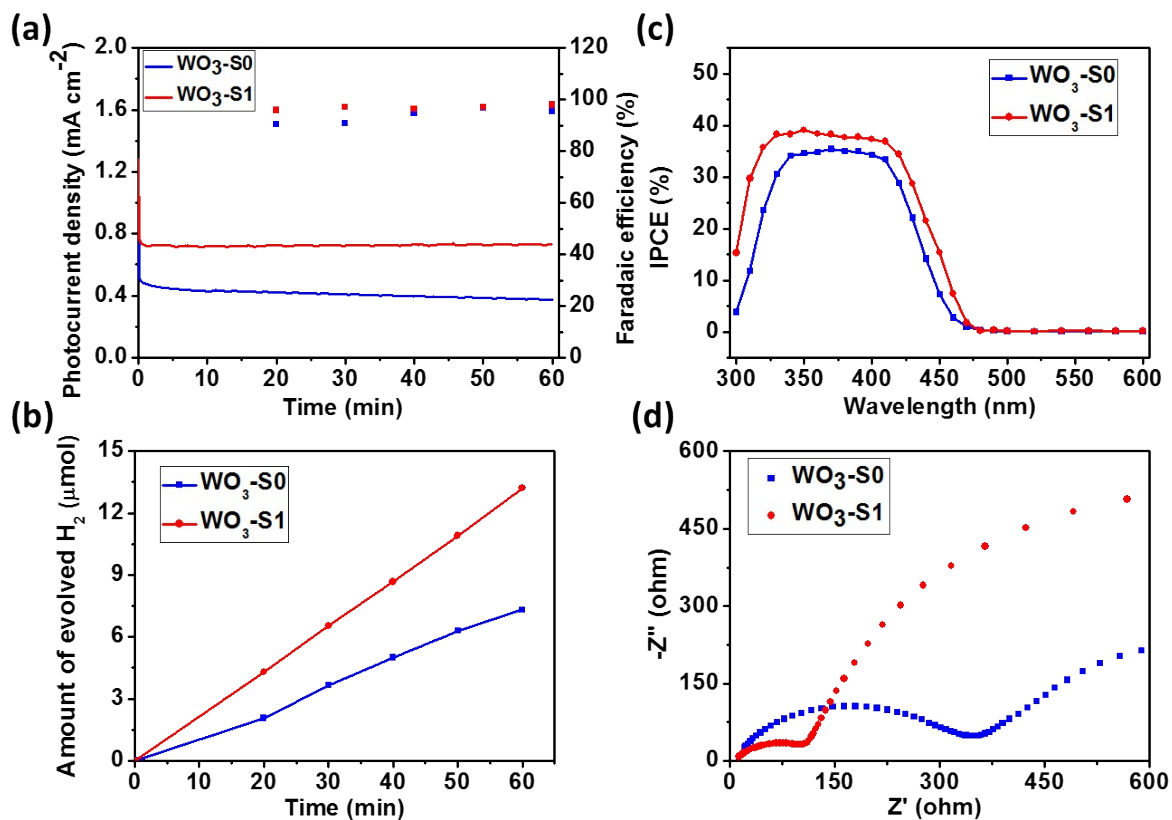


Figure S5 The *i-t* curves and relative faradaic efficiency (a) and the amount of evolved H₂ production (b) of WO₃-S0 and WO₃-S1 samples at the potential of 1.51 V vs. RHE under illumination for 60 min. (c) The IPCE plots of WO₃-S0 and WO₃-S1 samples at 1.23 V vs. RHE from 300-600 nm. (d) EIS results of WO₃-S0 and WO₃-S1 samples at the potential of 1.0 V vs. RHE with the frequency range from 0.1 Hz to 10 kHz under illumination.

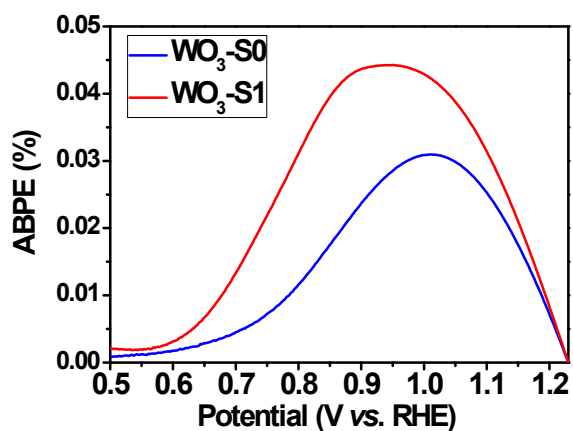


Figure S6 The applied bias photon-to-current efficiency (ABPE) of the samples.

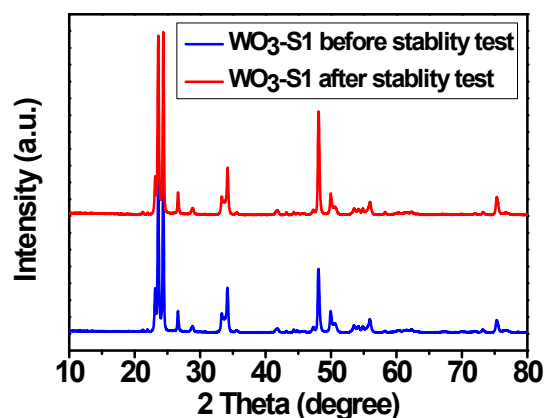


Figure S7 XRD patterns of $\text{WO}_3\text{-S1}$ before and after 24 hours stability test.

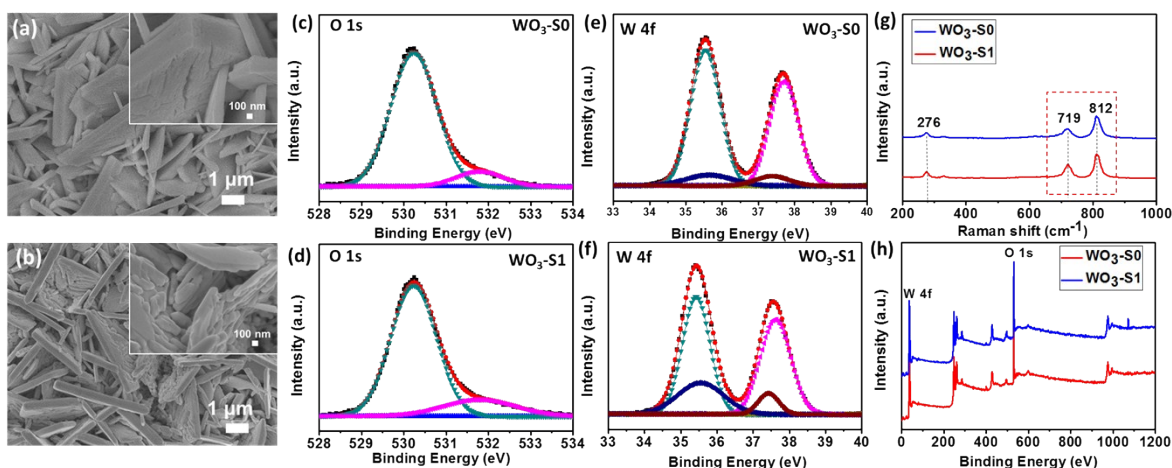


Figure S8 SEM images of the $\text{WO}_3\text{-S0}$ (a), and $\text{WO}_3\text{-S1}$ (b) after 24 hours stability test. The inserts are the corresponding high magnification images of above samples. O 1s (c, d) and W 4f (e, f) XPS spectra of the $\text{WO}_3\text{-S0}$ (c,e) and $\text{WO}_3\text{-S1}$ (d, f) samples after 24 hours stability test. (g) The room temperature Raman spectra of $\text{WO}_3\text{-S0}$ and $\text{WO}_3\text{-S1}$ samples after 24 hours stability tests. (h) The full survey spectra of XPS measurements of $\text{WO}_3\text{-S0}$ and $\text{WO}_3\text{-S1}$ after 24 hours stability tests.

Raman spectra of tested WO_3 samples show that monoclinic WO_3 structure also has negligible change after long-term tests (Figure S8g). Importantly, the intensity ratio of 719 to 812 cm^{-1} band of tested $\text{WO}_3\text{-S0}$ decreases to 0.5993, while it increases to 0.6889 for tested $\text{WO}_3\text{-S1}$. It is interesting that these changes in the band ratio is the same as the photocurrent changes. This may suggest that the symmetric bending (W-O bending (δ)) of W and O atoms may be beneficial for the charge separation, and thus leads to the photocurrent increase after two-step annealing.

Table S2 Comparison of the PEC performance of as-prepared our catalysts and reported oxygen-deficient WO₃ and other photoanodes.

Photoanode	Photocurrent @1.23V vs. RHE	Photostability	ABPE @1.0V vs. RHE	Substrate	pH of Electrolyte	Light irradiation
WO ₃ -S1(This work)	0.54 mA cm ⁻²	24h	0.04%	W foil	0.5 M Na ₂ SO ₄ (pH= 5.16)	visible light (100 mW cm ⁻²)
Single-Crystalline WO ₃ Microplates(330 nm) ¹	0.5 mA cm ⁻²	–	–	FTO	phosphate buffer (pH= 7)	visible light (100 mW cm ⁻²)
Single-crystalline WO ₃ microplates(470 nm) ¹	0.9 mA cm ⁻²	–	–	FTO	phosphate buffer (pH= 7)	visible light (100 mW cm ⁻²)
Single-Crystalline WO ₃ Microplates(330 nm) ¹	1.3 mA cm ⁻²	–	–	FTO	phosphate buffer (pH= 7)	UV-vis irradiation
Single-crystalline WO ₃ microplates(470 nm) ¹	1.9 mA cm ⁻²	–	–	FTO	phosphate buffer (pH= 7)	UV-vis irradiation
WO _{3-x} nanorods supported Zn _{0.3} Cd _{0.7} S heterostructure ²	0.05 mA cm ⁻²	–	–	Ti foil	0.1 M Na ₂ SO ₄	visible light (2.8 mW cm ⁻²)
WO _{3-x} @TiO _{2-x} core-shell nanosheets(15 nm) ³	3.2 mA cm ⁻²	6h	–	FTO	0.5 M Na ₂ SO ₄ (pH= 6.8)	visible light (100 mW cm ⁻²)
WO ₃ plate-like films ⁴	0.78 mA cm ⁻²	2h(15% loss)	–	FTO	0.5 M H ₂ SO ₄	visible light
WO ₃ nanotubes grown by FVD ⁵	1.5 mA cm ⁻²	–	0.21%	–	0.5 M Na ₂ SO ₄	visible light (100 mW cm ⁻²)
WO ₃ /Fe ₂ O ₃ nanocomposites ⁶	2 mA cm ⁻²	4h	0.45%	FTO	0.5 M Na ₂ SO ₄	visible light (100 mW cm ⁻²)
Nanostructured WO ₃ with triton surfactants ⁷	2 mA cm ⁻²	–	0.6%	FTO	1 M H ₂ SO ₄ (pH = 0)	visible light (100 mW cm ⁻²)

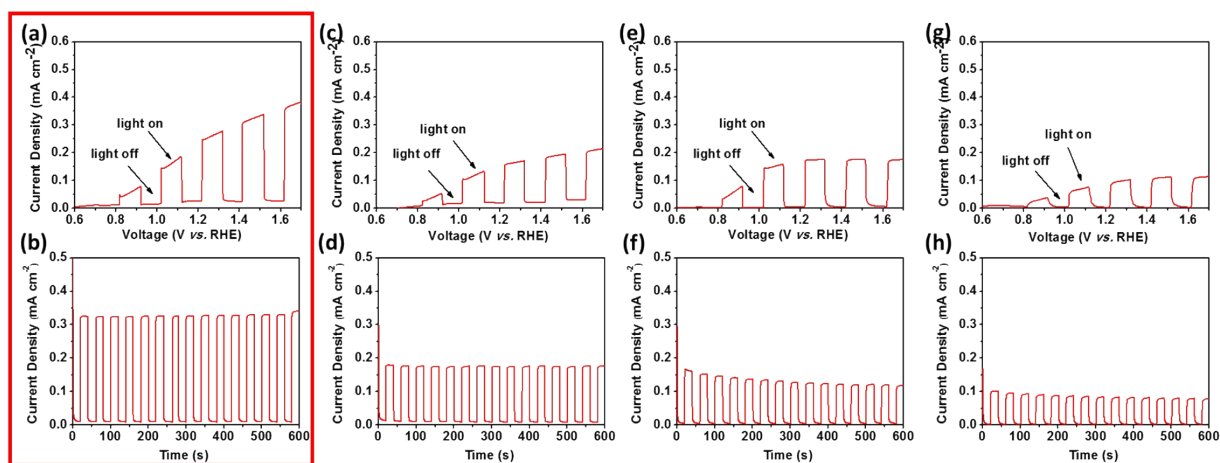


Figure S9 LSV curves and stability tests of WO_3 photoanodes first annealed at 550°C for 3 hours (a, b), 4 hours (c, d), 5 hours (e, f), and 6 hours (h, g), respectively. The LSVs are tested at scan rate = 10 mV s^{-1} under incident chopped light ($f = 0.1 \text{ Hz}$). The stability tests are tested at 1.51 V vs. RHE under incident chopped light ($f = 0.05 \text{ Hz}$).

Figure S9a-g show the LSV curves of WO_3 samples only experience conventional one-step annealing at 550°C for different duration (3-6 hours). The samples annealed for 3 hours, 4 hours, 5 hours, and 6 hours deliver a photocurrent of 0.25 , 0.16 , 0.16 , and 0.09 mA cm^{-2} at 1.23 V vs. RHE , respectively. The photocurrent of above four samples is sequentially decreasing according to the first annealing duration. At the same time, the 3 hours sample has the highest photocurrent together with the highest photocurrent retention in comparison with other three samples during the short-term stability tests (Figure S9b-h). It can be concluded that the 3 hours sample exhibits the highest photocurrent and best stability. Here, this is another reason that sample annealed at 550°C for 3 hours is chosen as $\text{WO}_3\text{-S0}$ and make further treatment to obtain oxygen-deficient WO_3 ($\text{WO}_3\text{-S1}$).

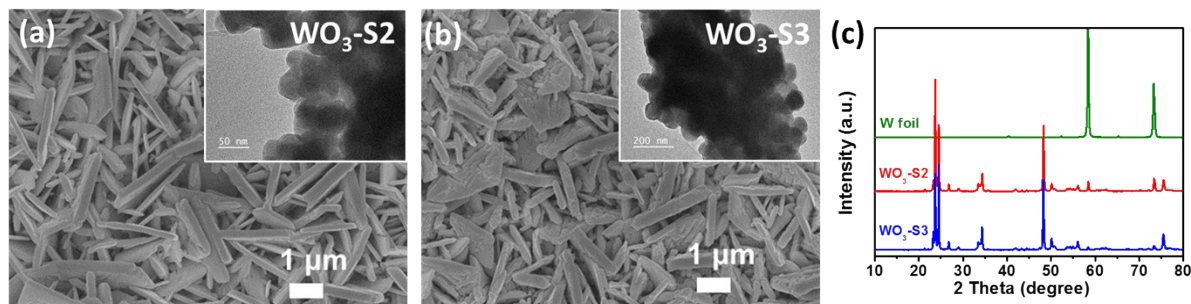


Figure S10 (a, b) SEM images about the WO_3 samples after a two-step annealing process. Here, the sample first annealed at 550°C for 3 hours, and then second annealed at 670°C for 30 min, and 700°C for 30 min, are denoted as $\text{WO}_3\text{-S2}$ (a) and $\text{WO}_3\text{-S3}$ (b), respectively. The inserts are the corresponding high magnification TEM images of above samples. (c) XRD patterns of the as-grown $\text{WO}_3\text{-S2}$ and $\text{WO}_3\text{-S3}$.

To make a supplement, the samples second annealed at 670°C for 30 min, 700°C for 30 min, are denoted as $\text{WO}_3\text{-S2}$ and $\text{WO}_3\text{-S3}$, respectively. After the second annealing process, the plate-like morphology of $\text{WO}_3\text{-S2}$ and $\text{WO}_3\text{-S3}$ do not show significant changes compared with $\text{WO}_3\text{-S0}$ and $\text{WO}_3\text{-S1}$. Both $\text{WO}_3\text{-S2}$ and $\text{WO}_3\text{-S3}$ plates contain rough surface and they are covered by particles. From TEM images, it is confirmed again that numerous particles distribute on the surface and there are distinct voids in-between those particles. The diameter of the particles is in the range of 40-100nm. As shown in XRD patterns, the diffraction peaks at 58° and 73° are indexed to the tungsten metal (JCPDS 04-0806), which is belonging to the W foil substrate. It is highly visible that the tungsten metal peaks of $\text{WO}_3\text{-S2}$ are quite weak. As the temperature increases to 700°C for 30 min, $\text{WO}_3\text{-S3}$ almost does not show the tungsten diffraction peaks. It can be concluded that the tungsten peaks are decreased and even vanished with higher temperature and longer duration of the second annealing process. Exclude the tungsten peaks, all the diffraction peaks are matched well with the monoclinic phase WO_3 (JCPDS 43-1035) and no second phase is observed.

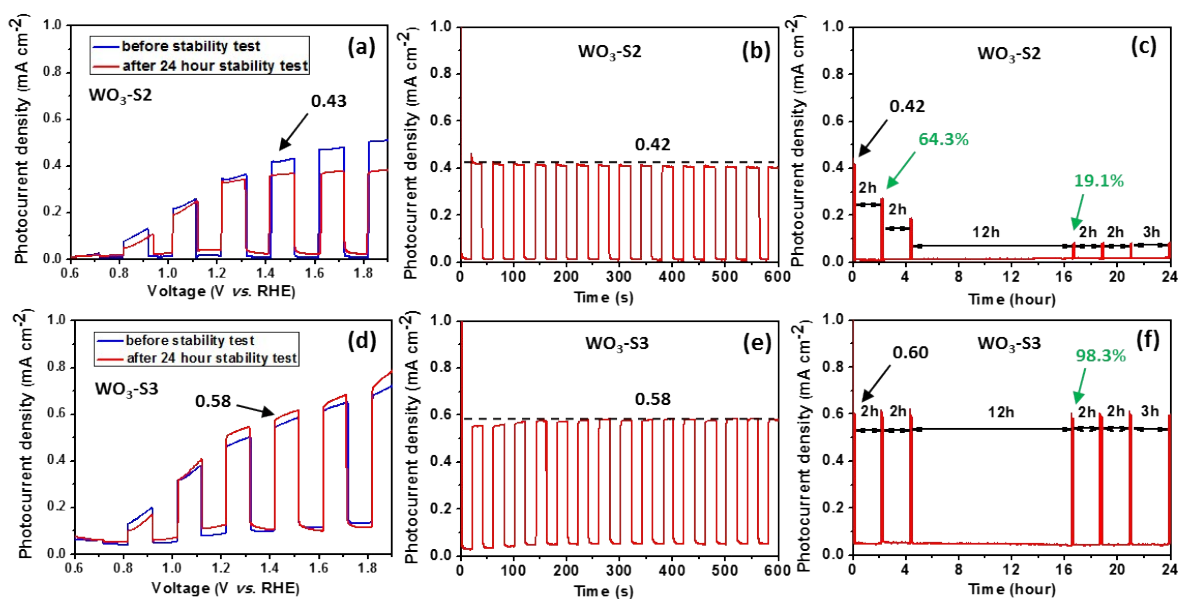


Figure S11 (a) LSV curves of $\text{WO}_3\text{-S2}$ in a three-electrode quartz glass system with 0.5 M Na_2SO_4 as the electrolyte. LSV tests are performed at 10 mV s^{-1} under incident chopped light ($f = 0.1 \text{ Hz}$, AM 1.5). The curves in blue are tested before stability test. The curves in red are tested after 24 hours stability test. (b) Short-term and (c) long-term stability tests of $\text{WO}_3\text{-S2}$ sample at a constant voltage of 1.51 V vs. RHE for 600s and 24 hours, respectively. Short-term stability tests are measured under incident chopped light ($f = 0.05 \text{ Hz}$, AM 1.5). Then, the above samples are used to perform the long-term stability tests with chopped light ($f = 0.05 \text{ Hz}$, AM 1.5) for 600s every 2 hours or 12 hours, and tested for 24 hours in total. (d) LSV curves, short-term and (e), and long-term (f) stability tests of $\text{WO}_3\text{-S3}$ sample in the same condition as $\text{WO}_3\text{-S2}$ sample.

Compared with $\text{WO}_3\text{-S0}$, two-step annealed $\text{WO}_3\text{-S2}$ and $\text{WO}_3\text{-S3}$ also show higher photocurrent density. After the second annealed at 670°C for 0.5 hour, the LSV photocurrent density of $\text{WO}_3\text{-S2}$ at 1.51 V vs. RHE increases to 0.43 mA cm^{-2} . When we proceeds to 700°C for 0.5 hour, the photocurrent density of $\text{WO}_3\text{-S3}$ increases to 0.58 mA cm^{-2} . However, their photocurrents is lower than that of $\text{WO}_3\text{-S1}$ (700°C for 1 hour). This indicates that the increase of photocurrent density may be attributed to the two-step annealing process, especially those treated in higher temperature and longer duration, leading to higher concentration of oxygen defects, and resulting in the higher charge generation. In the meantime, the short-term stability tests behave similar as $\text{WO}_3\text{-S0}$ and $\text{WO}_3\text{-S1}$, all the samples are stable in the short period. However, the photocurrent of $\text{WO}_3\text{-S2}$ decreases rapidly down to 0.08 mA cm^{-2} after 24 hours long-term test. Interestingly, when the long-term test is over, and another LSV test is conducted, the photocurrent of $\text{WO}_3\text{-S2}$ recovers back to 0.37 mA cm^{-2} . This phenomenon also can be find in

WO₃-S0, which may due to the inefficient charge separation of samples. However, for higher temperature (700°C) annealed WO₃-S1 and WO₃-S3, there is no such decrease and recovering changes in photocurrent. Although there is a photocurrent increase of both WO₃-S1 and WO₃-S3, originating from that excessive oxygen defects gradually get involved in the photoelectrochemical reaction during long-term tests.

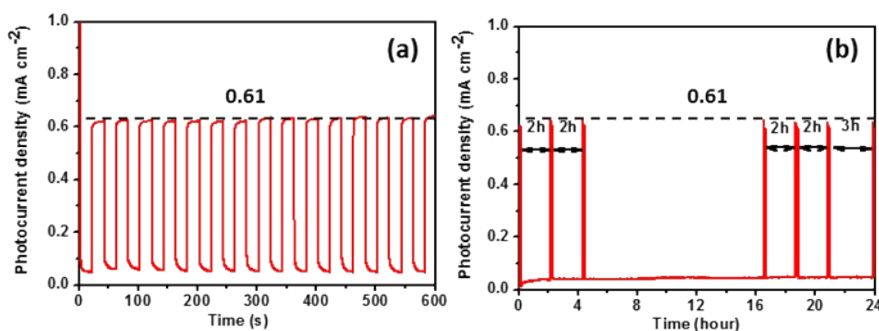


Figure S12 (a) Short-term stability test of WO₃-S3 sample for 600s after the first 24h stability test. (b) Another 24h long-term stability test of WO₃-S3 sample after the first 24h long-term and short-term stability tests. All the stability tests are measured at a constant voltage of 1.51 V vs. RHE under incident chopped light ($f = 0.05$ Hz, AM 1.5).

We continue with another 600s short-term and a 24 hours long-term stability test on WO₃-S3 sample (the same device). Here, the photocurrent of WO₃-S3 is as high as 0.61 mA cm⁻², and it almost has no photocurrent loss during these two measurements. It can be concluded that photocurrent is higher and much more stable with high temperature/long duration annealed WO₃ samples as compared to WO₃-S0 and WO₃-S2.

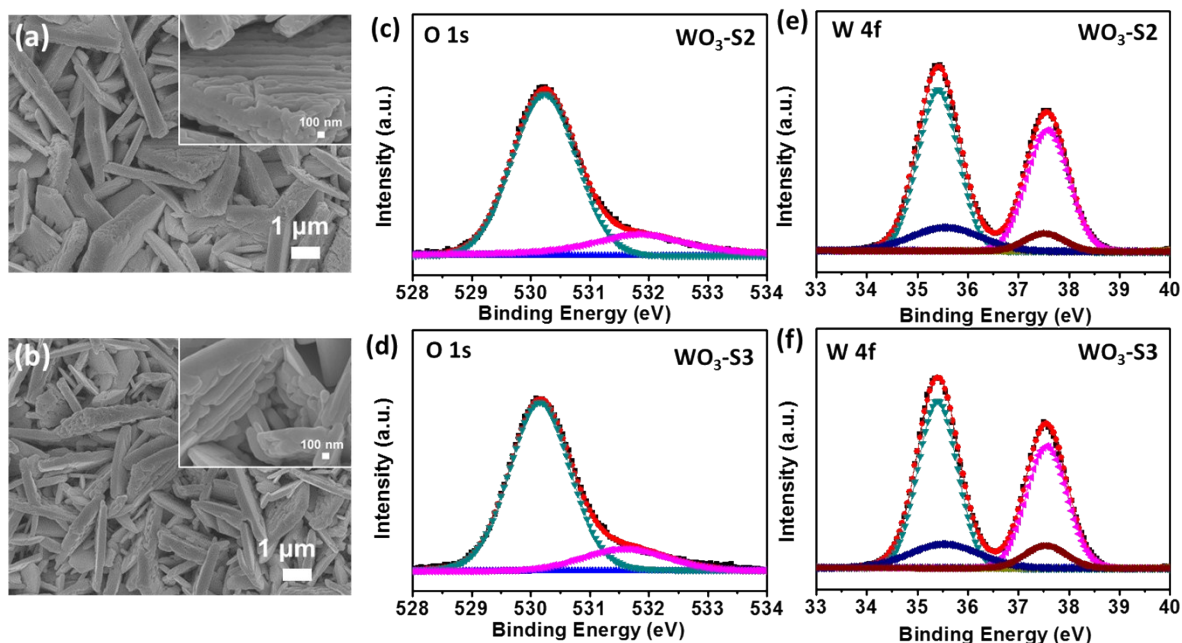


Figure S13 SEM images of the $\text{WO}_3\text{-S2}$ (a), and $\text{WO}_3\text{-S3}$ (b) after 24 hours stability test. The inserts are the corresponding high magnification images of the above samples. The scale bar corresponds to 1 μm (big images) and 100 nm (insert images). O 1s (c, d) and W 4f (e, f) XPS spectra of the $\text{WO}_3\text{-S0}$ (c,e) and $\text{WO}_3\text{-S1}$ (d, f) samples after 24 hours stability test.

The morphologies of $\text{WO}_3\text{-S2}$ and $\text{WO}_3\text{-S3}$ after 24 hours stability tests are recorded in Figure S13. In comparison with as-grown samples, the tested samples almost stay unchanged, still preserve the plate-like structure and cover with particles. Additionally, the XPS patterns of tested $\text{WO}_3\text{-S2}$ and $\text{WO}_3\text{-S3}$ samples show that the surface chemical states do not change much after long-term tests.

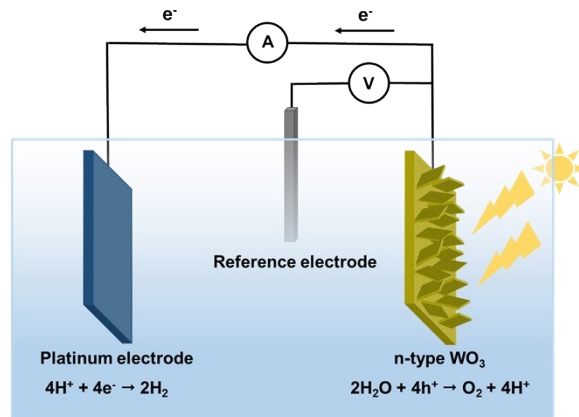


Figure S14 Schematic diagram of basic components of PEC cell with the plate-like WO_3 photoanode and a Pt cathode.

The WO_3 samples together with platinum electrode and reference electrode are assembled into PEC cell to investigate their photoelectrochemical performance.

References:

1. M. Park, J. H. Seo, H. Song and K. M. Nam, *The Journal of Physical Chemistry C*, 2016, **120**, 9192-9199.
2. A. B. Yousaf, M. Imran, S. J. Zaidi and P. Kasak, *Scientific Reports*, 2017, **7**, 6574.
3. K. Yuan, Q. Cao, H.-L. Lu, M. Zhong, X. Zheng, H.-Y. Chen, T. Wang, J.-J. Delaunay, W. Luo, L. Zhang, Y.-Y. Wang, Y. Deng, S.-J. Ding and D. W. Zhang, *Journal of Materials Chemistry A*, 2017, **5**, 14697-14706.
4. Y. Liu, J. Li, H. Tang, W. Li, Y. Yang, Y. Li and Q. Chen, *Electrochemistry Communications*, 2016, **68**, 81-85.
5. P. M. Rao, I. S. Cho and X. Zheng, *Proceedings of the Combustion Institute*, 2013, **34**, 2187-2195.
6. A. Memar, C. M. Phan and M. O. Tade, *International Journal of Hydrogen Energy*, 2015, **40**, 8642-8649.
7. A. Memar, C. M. Phan and M. O. Tade, *Applied Surface Science*, 2014, **305**, 760-767.